



Changes in the macro and nano-structure of paper during moisture cycling

Per Tomas Larsson · Johan Alfthan ·
Galya Simeonova · Claes Holmqvist

Received: 28 February 2023 / Accepted: 14 November 2023 / Published online: 20 December 2023
© The Author(s) 2023

Abstract Hygroexpansion, CP/MAS ^{13}C -NMR, WAXS and SAXS measurements were carried out on sheets made from four different commercial pulps of varying lignin content. Non-directional laboratory sheets were made at different press levels from the pulps following different degrees of beating. The sheets were dried both freely and with restraints. Measurements were made on sheets before and after moisture cycling to determine hygroexpansion coefficients, changes in cellulose average lateral fibril dimensions and average cellulose crystallite sizes, with the aim of understanding macroscale and nanoscale changes as the result of moisture cycling. Within the sheets consistent and statistically significant structural changes were observed on both macro and nanoscale. On the macroscale, moisture cycling consistently induced irreversible shrinkage in sheets dried with restraints, but less so in the case of sheets dried freely. The hygroexpansion coefficients were typically higher for freely dried sheets compared with sheets dried with constraints. On the nanoscale,

moisture cycling consistently caused an increase in the average crystallite sizes (WAXS) and the average lateral fibril dimensions (CP/MAS ^{13}C -NMR), though the latter occurred with poor statistical significance. These changes were interpreted as an increase in the degree of order in the cellulose fibril interior/cellulose crystallite. There were no profound differences in the nanoscale changes observed for sheets dried with restraints and for sheets dried freely. Changes in the fibre wall nanostructure were of similar magnitudes when comparing results from freely dried low grammage sheets (less abundant inter-fibre joints) with freely dried sheets of higher grammage (more abundant inter-fibre joints). No obvious correlations were found between the macroscale and nanoscale measurements. The proposed explanation for this was that the nanoscale structural changes occurred similarly throughout the entirety of the fibre wall, independent of the proximity to an inter-fibre joint, and that the nanoscale structural changes were mainly the result of water penetrating into the interior of cellulose fibril aggregates. By using the same fibril model for evaluation of CP/MAS ^{13}C -NMR and WAXS data, good-to-reasonable agreement were found for estimates of the degree of cellulose crystallinity.

This article is part of a collection of articles in honor of Dr. Henri Chanzy on the occasion of his 90th birthday. The article was not finished in time to be bound with the rest of the papers in the Special Issue #13, September, 2023.

P. T. Larsson (✉) · J. Alfthan · G. Simeonova ·
C. Holmqvist
RISE AB, Drottning Kristinas Väg 61, 114 86 Stockholm,
Sweden
e-mail: tomas.larsson@ri.se

Keywords Liner · Kraft pulp · Bleached pulp ·
Hygroexpansion · Moisture cycling · WAXS · SAXS ·
CP/MAS ^{13}C -NMR · Nanostructure · Macrostructure

Background

Wood pulps are a renewable commodity produced world-wide in large volumes for use in paper and paperboard. The global production capacity of wood pulps for paper and paperboard was estimated at 157 million tonnes in 2021 (FAO 2017). Chemical wood pulps are composed of separated anatomical plant fibres enriched in cellulose. The fibre wall of a pulp fibre contains enriched cellulose I in a complex hierarchical arrangement (Fengel and Wegener 1989), with cavities (or pores) resulting from complete or partial removal of lignin and hemicelluloses.

Production of paper and paperboard is accomplished by wet-forming a network of pulp fibres followed by drying that consolidates the network and allows for the development of inter-fibre joints. Tailoring quality for different end-uses is typically achieved by choice of pulp type and by controlling the grammage of the final paper/board. A common feature of both paper and paperboard is the hierarchical nature of the material. Specifically, the wall of an individual fibre is composed of a network of cellulose fibrils (after partial lignin and hemicellulose depletion). These fibres then constitute the building blocks for a larger sheet-network of conjoined fibres, within paper and paperboard products. The macroscopic strength properties of a paper sheet are the result of the individual fibre strength in combination with the strength and abundance of inter-fibre joints (Niskanen and Kärenlampi 1998).

The pulp fibres and paper sheets made thereof are hygroscopic and their properties are susceptible to moisture (Kajanto and Niskanen 1998). At high humidity the moisture in the paper or paperboard increases, causing the mechanical properties like stiffness and strength to deteriorate. Dimensional stability is also compromised when humidity changes. Paper materials expand when humidity increases and shrink when it decreases. This behaviour is known as hygroexpansion.

The lack of dimensional stability causes problems during converting of paper and paperboard into packaging and printed products. During the converting processes it is seldom possible to keep moisture constant due to e.g., printing or gluing. Dimensional changes during the converting could lead to registration errors in printing, or mismatch in dimensions when papers or boards are cut and folded into

packaging, resulting in problems during production as well as poor or non-functional products.

The dimensional changes can be irreversible, leading to permanent changes in shape, including curling or twisting of an originally flat paper or paperboard. The irreversible dimensional changes typically occur as a transient effect when the paper material is exposed to high humidity levels. The transient behaviour vanishes with repeated cycling of humidity. The transient effects are attributed to release of internal residual stresses in the material and is highly dependent on the constraints and stresses applied during the drying of the paper when it was produced (Kajanto and Niskanen 1998). In a hierarchical structure such as a paperboard, it is difficult to identify the exact causes for the permanent dimensional changes, i.e., if dimensional changes are mainly caused by the breaking and reformation of inter-fibre joints or if they mainly originate from changes in the fibre wall interior or if it is a combination of several factors.

X-ray scattering studies on wood has shown that repeated wetting and drying induce permanent change in the wood nanostructure e.g. increasing cellulose crystallite sizes (Toba et al. 2013). In the same study it was also observed that cellulose samples of high purity, Avicel powder, showed smaller changes in nanostructure in response to repeated drying and wetting. Wood based pulps obtained at different processing stages can be viewed as intermediates between wood and Avicel, with respect to cellulose purity and structure. It would therefore be interesting to find out if, and to what extent, changes observed in wood, also exist in pulps of at different processing stages.

To address this issue, this study focused on assessing if permanent structural changes could be observed in the fibre wall interior, as the result of exposing paper sheets to cyclic humidity changes. CP/MAS ¹³C-NMR, WAXS and SAXS were used to measure the fibre wall interior of paper before and after exposure to moisture cycling, during which the permanent macroscopic dimensional changes of the paper was recorded. To the best of the authors knowledge, deploying both NMR spectroscopy and x-ray scattering for addressing nanostructural changes in wood pulps during moisture cycling has not been previously reported.

Table 1 Pulp types, names, and wood composition of the used pulps

Pulp type	Abbreviation	Wood composition (Spruce/Pine)
Liner pulp	L1nd	35%/65%
Unbleached pulp	U1nd	60%/40%
Oxygen delignified pulp	O1nd	60%/40%
Bleached pulp	B1nd	60%/40%

Experimental

Materials: Four never-dried commercial pulps made from Scandinavian softwood were used in this study, Table 1.

The U1nd, O1nd and B1nd pulps were taken from the same fibre line with sampling delays matched to the production rate, for the purpose of obtaining unbleached, oxygen delignified and bleached pulp samples originating from the same fibre material. The L1nd was obtained from another pulp mill.

Sample identity syntax: Pulps were subjected to different degrees of beating, different press-levels and dried freely or with constraints prior to measurements. The sample naming syntax used throughout this work is illustrated by the following examples:

Example 1: L1nd-0P1R: (L) Liner pulp, (1) ID no. 1, (nd) never-dried, (0) unbeaten, (P1) press-level 1, (R) dried with restraints, NMR/SAXS/WAXS measurement were made before moisture cycling.

Example 2: U1nd-190P3F_h: (U) unbleached pulp, (1) ID no. 1, (nd) never-dried, (190) beating energy 190 kWh/tonne, (P3) press-level 3, (F) dried freely, (_h) NMR/SAXS/WAXS measurement were made after moisture cycling.

Example 3: B1nd-0P4F-T_h: (B) bleached pulp, (1) ID no. 1, (nd) never-dried, (0) unbeaten, (P4) press-level 4, (F) freely dried, (T) a low grammage tissue sheet, (_h) NMR/SAXS/WAXS measurement made after moisture cycling.

Chemical composition: Carbohydrate composition was determined according to SCAN-CM 71:09 using a high-performance anion-exchange chromatography system, Dionex ISC-5000, coupled to a CarboPac PA1 (250 mm × 4 mm i.d.) column (Dionex, Sweden) and a pulsed amperometric detector (HPAEC-PAD). The xylan, glucomannan and cellulose contents were calculated from the monosaccharides according to

Jansson (1974). The acid insoluble (Klason) lignin was determined according to Tappi T222 and acid soluble lignin according to Tappi UM 250.

Pulp treatments: The pulps were beaten (refined) using a Voith LR40 laboratory refiner equipped with conical softwood fillings (bar width 3.0 mm, groove width 12 mm, mean cutting angle 60°, cutting edge length 0.02 km/revolution). During the beating, the pulp was recirculated until the target refining energy input level (i.e., the employed refining energy per mass of dry pulp) was reached. Some samples were prepared from unbeaten pulp. To ensure good dispersion of the pulp material, the pulp was then given a gentle mechanical treatment in a laboratory disintegrator prior to use. The result of the refining was characterized by measuring the Schopper-Riegler drainage resistance of the beaten pulps (SR, ISO 5267–1). The fibre length distribution was measured for all pulps using a L&W Fiber Tester Plus instrument (AB Lorentzen & Wettre, Stockholm, Sweden, whole pulp setting).

Sample sheet preparation: Non-directional laboratory sheets with a (bone dry) basis weight of 100 g/m² were formed according to SCAN-CM 64, with a modified wet pressing procedure. To ensure that the composition of the sample sheets equals the composition of the pulp, a series of 10 sheets were made with recirculation of the drained water before the actual sample sheets were produced. The initial sheets were discarded. The formed sheets were wet pressed between blotting papers using different pressures. The label P1 refers to pressing at 200 kPa for 5 min, while P3 refers to pressing at 410 kPa for 5 min after which the blotting papers were changed and the sheets pressed for an additional 2 min. The different procedures were used to obtain sheets with different densities. The sheets were either dried under restraints preventing any lateral shrinkage (SCAN-CM 64), or according to a procedure allowing approximately free lateral shrinkage. For both restrained and free drying, the sheets were allowed to dry in a conditioned room (temperature 23 °C, RH 50%). In the latter case, the pressed sheets were placed between two low-friction PEEK fabrics, which were put on a somewhat curved metal surface, and covered with a slightly tensioned textile cloth. This arrangement resulted in essentially flat sheet samples i.e., with a tolerable degree of out of plane deformations that would not significantly interfere with subsequent measurements. As a

reference, a few sheets were placed on a Teflon surface and allowed to dry without any prevention of out of plane deformations. The lateral shrinkage of these sheets, which had a very non-flat shape, was somewhat larger than for the sheets dried between two low-friction PEEK fabrics, but the difference was small enough that the sheets dried between the PEEK fabrics may be considered approximately freely dried. For example, a 100 g/m² sheet from bleached Kraft pulp refined to 300 kWh/t exhibited 6.7% shrinkage when dried on the Teflon surface, and 4.8% shrinkage when dried between the PEEK fabrics. In addition to the 100 g/m² laboratory sheets, a few sheets with (bone dry) weight 10 g/m² were made from the pulps L1nd and B1nd for complementary measurements in WAXS, SAXS and CP/MAS ¹³C-NMR. These sheets were similar to tissue papers. The difference from the

higher grammage sheets demanded a few changes in the manufacturing procedure. Only unbeaten pulps were used. Pressing between blotting papers was performed at 410 kPa for 5 min, and labelled P4. The sheets were then allowed to dry completely freely without any prevention of out of plane deformations, which consequently became quite large. Table 2 shows papermaking parameters for the different sheet samples. Schopper-Riegler (SR) measures the rate of drainage of a diluted pulp suspension and indicates the degree of work done on the fibres during stock preparation. The specific edge load (SEL) is a measure of the intensity of the refining.

Hygroexpansion measurements: The RISE Hygroexpansivity Tester is designed for measurement of in-plane hygroexpansion of paper. It consists of a closed chamber equipped with mounting positions for 30 test

Table 2 Papermaking parameters for the different samples: Pulp type, refining energy and specific edge load (SEL), pulp concentration during refining, Schopper-Riegler of the pulp (SR), press level and type of restraint during drying

Sample	Pulp	Energy (kWh/t)	SEL (J/m)	Conc. (%)	SR	Press level	Drying
L1nd-0P1R L1nd-0P1F	Liner Kraft, never dried	0	2.5	–	13	P1	Rest. Free
L1nd-0P3R L1nd-0P3F	Liner Kraft, never dried	0	2.5	–	13	P3	Rest. Free
L1nd-0P4F-T (tissue sheets)	Liner Kraft, never dried	0	2.5	–	13	P4	Free
L1nd-300P1R L1nd-300P1F	Liner Kraft, never dried	300	2.5	–	23	P1	Rest. Free
L1nd-300P3R L1nd-300P3F	Liner Kraft, never dried	300	2.5	–	23	P3	Rest. Free
U1nd-0P1R U1nd-0P1F	Unbleached Kraft, never dried	0	2.5	3.5	13	P1	Rest. Free
U1nd-0P3R U1nd-0P3F	Unbleached Kraft, never dried	0	2.5	3.5	13	P3	Rest. Free
U1nd-190P1R U1nd-190P1F	Unbleached Kraft, never dried	190	2.5	3.5	23	P1	Rest. Free
U1nd-190P3R U1nd-190P3F	Unbleached Kraft, never dried	190	2.5	3.5	23	P3	Rest. Free
O1nd-0P1R O1nd-0P1F	Oxygen delignified, never dried	0	2.5	3.5	14	P1	Rest. Free
O1nd-0P3R O1nd-0P3F	Oxygen delignified, never dried	0	2.5	3.5	14	P3	Rest. Free
O1nd-150P1R O1nd-150P1F	Oxygen delignified, never dried	150	2.5	3.5	23	P1	Rest. Free
O1nd-150P3R O1nd-150P3F	Oxygen delignified, never dried	150	2.5	3.5	23	P3	Rest. Free
B1nd-0P1R B1nd-0P1F	Bleached Kraft, never dried	0	2.0	4.5	14	P1	Rest. Free
B1nd-0P3R B1nd-0P3F	Bleached Kraft, never dried	0	2.0	4.5	14	P3	Rest. Free
B1nd-0P4F-T (tissue sheets)	Bleached Kraft, never dried	0	2.0	4.5	14	P4	Free
B1nd-100P1R B1nd-100P1F	Bleached Kraft, never dried	100	2.0	4.5	17	P1	Rest. Free
B1nd-100P3R B1nd-100P3F	Bleached Kraft, never dried	100	2.0	4.5	17	P3	Rest. Free
B1nd-180P1R	Bleached Kraft, never dried	180	2.0	4.5	23.5	P1	Rest
B1nd-180P3R	Bleached Kraft, never dried	180	2.0	4.5	23.5	P3	Rest

pieces. The humidity in the chamber is controlled by an external humidity generator. The test pieces are paper strips, which are 15 mm wide and have a clamping length of 100 mm. The test pieces are placed on a horizontal low-friction table and mounted between two aligned clamps for each test piece position. One of the clamps has a fixed position, while the other clamp is mounted on a smooth-running horizontal sled allowing it to move when the test piece changes its length due to hygroexpansion. A traversing CCD laser displacement sensor is used to measure the position of the moving sleds for each test piece. When the measurements are performed, a pneumatically controlled dynamic anti-buckling device is temporarily applied to flatten the test pieces to ensure that the correct length is measured. The hygroexpansion strains ϵ can then be determined from the change in length ΔL and the original length L_0 according to Eq. 1:

$$\epsilon = \frac{\Delta L}{L_0} \quad (1)$$

When not measuring the length, the test pieces are free, exposing them to the surrounding humidity and allowing them to change dimension without interference. Additional test pieces from the tested papers are kept in the chamber to be conditioned to the same climate. From these, the moisture ratio was determined gravimetrically. The moisture ratio was determined from the mass of the paper at the current relative humidity M and the mass of completely dry paper M_d , Eq. 2:

$$m_r = \frac{M - M_d}{M_d}. \quad (2)$$

The mass of the completely dry paper M_d was obtained after oven drying of the test pieces when the hygroexpansion test had been completed. In the present study, a relative humidity (RH) cycle of 50%–20%–90%–50% was repeated 4 times while the temperature was kept at 23 °C. At each level, the RH was held constant for at least 24 h to ensure that the moisture ratio of the test pieces had reached equilibrium. Hygroexpansion strains and moisture ratios were determined at the end of this period. At least 5 test pieces for each paper were used to determine the hygroexpansion strains, and at least 4 test pieces were used to determine the moisture ratios.

During the relative humidity cycling, the hygroexpansion will show a transient initial behaviour when the humidity is increased for the first time, and a stabilisation in the dimensional changes during the following cycles. During the final humidity cycles, the hygroexpansion is reversible and close to linear with respect to the moisture ratio. A hygroexpansion coefficient β can be defined as the ratio between the change in hygroexpansion strain $\Delta\epsilon$ and the change in moisture ratio Δm_r , Eq. 3:

$$\beta = \frac{\Delta\epsilon}{\Delta m_r}. \quad (3)$$

When the hygroexpansion has stabilised to a linear behaviour during the final cycles, the hygroexpansion coefficient β is a macroscopic material property of the paper material. In this work, the hygroexpansion coefficient was evaluated both during the first cycle using the first increase from the lowest to the highest relative humidity, i.e., from 20% RH to 87% RH, and during the final cycle using the last increase from the lowest to the highest relative humidity. These hygroexpansion coefficients were denoted β_{init} and β_{final} respectively. The permanent change in dimensions from the starting point at 50% RH to the end point of the 4 cycles at 50% was also determined. The change was expressed as an irreversible shrinkage, denoted ϵ_{irr} .

X-ray scattering: X-ray measurements were performed on an Anton Paar SAXSpoint 2.0 system (Anton Paar, Graz, Austria) equipped with a Microsource x-ray source (Cu K α radiation, wavelength 0.15418 nm) and a Dectris 2D CMOS Eiger R 1M detector with 75 μ m by 75 μ m pixel size. All measurements were performed with a beam size of about 500 μ m in diameter, at a sample stage temperature of 25 °C with a beam path pressure at 1–2 mBar. For SAXS measurements, the sample to detector distance (SDD) was 563 mm and for WAXS measurements the SDD was 111 mm. Samples were mounted in the sample holder as sheets. Water swollen samples were mounted on a Multi-paste Holder mounted on a Heated Sampler and a VarioStage (Anton Paar, Graz, Austria). Water swollen samples were kept between Kapton foils in hermetically sealed compartments and were not exposed to vacuum during measurement. Dry samples were mounted on a Solids Sampler Holder mounted on a VarioStage (Anton Paar,

Table 3 Relative chemical composition of the pulps

Substance (%)	L1nd	U1nd	O1nd	B1nd
Xylan	9	9	9	8
(Galacto) Glucomannan	8	8	8	9
Cellulose	70	80	82	83
Lignin	12	3	1	0.3

Graz, Austria). The dry samples were exposed to the vacuum in the beam path. For wet samples, scattering data recorded on deionized water with the same experimental setup was used for background subtraction, an arbitrary scaling of the water signal was used. Binning was used to generate graphs with between 500 and 510 data points, which were used for graphs. For WAXS and SAXS samples, 6 frames each of 30 min duration were recorded, giving a total measurement time of 180 min per sample. For all samples, the transmittance was determined and used for scaling of the scattering intensities. The software used for instrument control was SAXSdrive version 2.01.224 (Anton Paar, Graz, Austria), and post-acquisition data processing was performed using the software SAXSanalysis version 3.00.042 (Anton Paar, Graz, Austria).

Crystallite sizes were obtained from WAXS measurements by an estimate of the full width at half maximum (FWHM) of the (200) signal by the Scherrer equation. To obtain the (200) FWHM, the WAXS

diffractogram was fitted, after background subtraction, using Gaussian functions. From the function describing the (200) signal the FWHM was calculated. The software used for fitting was the same as the one used for fitting NMR spectra (Larsson 1997).

To estimate the cellulose degree of crystallinity the same structural model was used for both CP/MAS ^{13}C -NMR and WAXS data. Based on the crystallite size obtained by the Scherrer equation, an estimate of the average lateral fibril dimension (*sLFD*), analogous to what is obtained from CP/MAS ^{13}C -NMR spectra, was estimated by the following formula:

$$sLFD = \frac{CS}{\sqrt{2}} + 1.14 \quad (4)$$

The assumption made in Eq. 4 is that the Scherrer crystallite size obtained from the (200) WAXS signal (*CS*) gives an estimate of the lateral diagonal of the fibril's crystalline core, discriminating contributions from the fibril surface polymers. *sLFD* is consequently computed by adding one polymer layer, with an approximate thickness of 0.57 nm (Krässig 1993) around the circumference of the crystallite core. With an estimate of the average lateral fibril dimensions, the estimate of the degree of crystallinity is obtained, analogous the procedure use for estimating the degree of cellulose crystallinity from CP/MAS ^{13}C -NMR spectra (Wickholm et al. 1998).

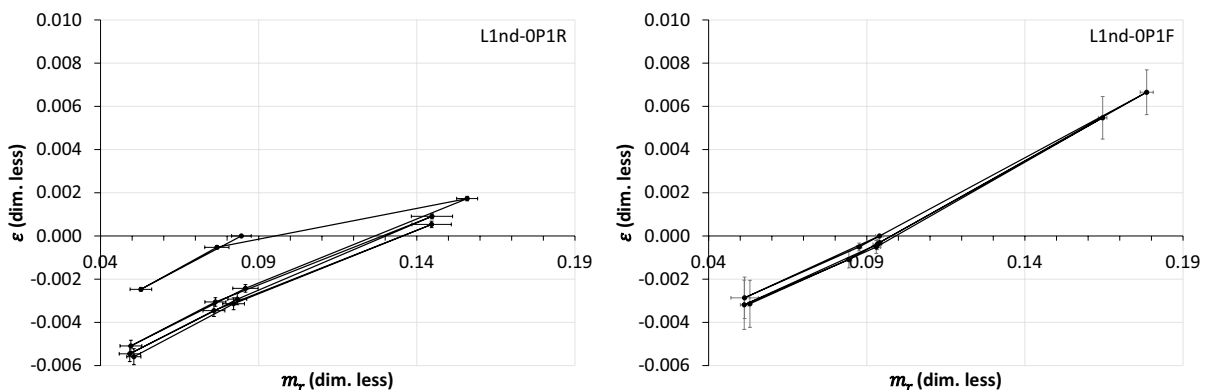


Fig. 1 Two examples of measurements of hygroexpansion strains (ϵ) as function of moisture ratio (m_r). Left panel: sample L1nd-OP1R showing a typical behaviour of restrained dried samples. Right panel: sample L1nd-OP1F showing typical behaviour of freely dried samples. The measurement starts

at a moisture ratio (m_r) corresponding to the initial 50% RH, in these cases between 0.08 and 0.10, and a hygroexpansion strain (ϵ) which is defined as zero (Eq. 1). Error bars indicate standard deviations

Table 4 Evaluated parameters from the hygroexpansion measurements for sheets dried with restraints: Initial hygroexpansion coefficient β_{init} , final hygroexpansion coefficient β_{final} , and irreversible shrinkage ϵ_{irr} . Values in brackets are standard deviations

Sample	$\beta_{init}(1)$	$\beta_{final}(1)$	$\epsilon_{irr}(1)$
L1nd-0P1R	0.0407 (0.0022)	0.0628 (0.0062)	0.0031 (0.0003)
L1nd-0P3R	0.0430 (0.0053)	0.0628 (0.0033)	0.0032 (0.0001)
L1nd-300P1R	0.0622 (0.0033)	0.0804 (0.0054)	0.0031 (0.0001)
L1nd-300P3R	0.0541 (0.0040)	0.0828 (0.0242)	0.0034 (0.0003)
U1nd-0P1R	0.0342 (0.0063)	0.0420 (0.0177)	0.0031 (0.0008)
U1nd-0P3R	0.0348 (0.0104)	0.0464 (0.0218)	0.0017 (0.0015)
U1nd-190P1R	0.0389 (0.0088)	0.0486 (0.0063)	0.0018 (0.0003)
U1nd-190P3R	0.0300 (0.0108)	0.0397 (0.0166)	0.0013 (0.0008)
O1nd-0P1R	0.0503 (0.0041)	0.0758 (0.0040)	0.0033 (0.0001)
O1nd-0P3R	0.0635 (0.0037)	0.0724 (0.0023)	0.0028 (0.0001)
O1nd-150P1R	0.0328 (0.0054)	0.0417 (0.0124)	0.0007 (0.0010)
O1nd-150P3R	0.0321 (0.0063)	0.0469 (0.0178)	0.0009 (0.0010)
B1nd-0P1R	0.0813 (0.0218)	0.0960 (0.0098)	0.0039 (0.0002)
B1nd-0P3R	0.0792 (0.0120)	0.1133 (0.0287)	0.0035 (0.0001)
B1nd-100P1R	0.0726 (0.0085)	0.0937 (0.0121)	0.0032 (0.0002)
B1nd-100P3R	0.0868 (0.0227)	0.1053 (0.0088)	0.0033 (0.0003)
B1nd-180P1R	0.0426 (0.0022)	0.0787 (0.0024)	0.0048 (0.0001)
B1nd-180P3R	0.0508 (0.0041)	0.0809 (0.0043)	0.0046 (0.0002)

For SAXS data, transmittance scaled data was further scaled to a fixed (arbitrary) value based on a numerical estimate of the ‘Porod invariant’ (Spalla 2002). The discrete estimate of the ‘Porod invariant’ (Q) used was, Eq. 5:

$$Q = \Delta q \sum_{i=1}^N I_i q_i^2 \quad (5)$$

where N is the number data points, I_i and q_i are the intensity and scattering vector respectively, and Δq the step size of the scattering vector (unit: nm^{-1}).

CP/MAS ^{13}C -NMR: Cross-Polarization Magic Angle Spinning Carbon-13 Nuclear Magnetic Resonance Spectra. All samples were packed uniformly in a zirconium oxide rotor. Water swollen samples had a water content of 40–60%. The CP/MAS ^{13}C -NMR spectra were recorded in a Bruker Avance III AQS 400 SB instrument operating at 9.4 T. All measurements were carried out at 295 (± 1) K with a magic angle spinning (MAS) rate of 10 kHz. A 4 mm double air-bearing probe was used. Data acquisition was performed using a cross-polarization (CP) pulse sequence, i.e., a 3.15 microseconds proton 90° pulse, 800 microseconds ramped (100–50%) falling contact pulse, with a 2.5 s delay between repetitions. A SPI-NAL64 pulse sequence was used for ^1H decoupling. The Hartmann-Hahn matching procedure was based on glycine. The chemical shift scale was calibrated to the TMS-scale (tetramethylsilane, $(\text{CH}_3)_4\text{Si}$) by assigning the data point of maximum intensity in the alpha-glycine carbonyl signal to a shift of 176.03 ppm. 4096 transients were recorded on each sample leading to an acquisition time of about 3 h. The software for spectral fitting was developed at RISE AB and is based on a Levenberg–Marquardt algorithm (Larsson 1997). All computations were based on integrated signal intensities obtained from spectral fitting (Wickholm 1998). The errors given for parameters obtained from the fitting procedure are the standard error with respect to the quality of the fit.

Results and discussion

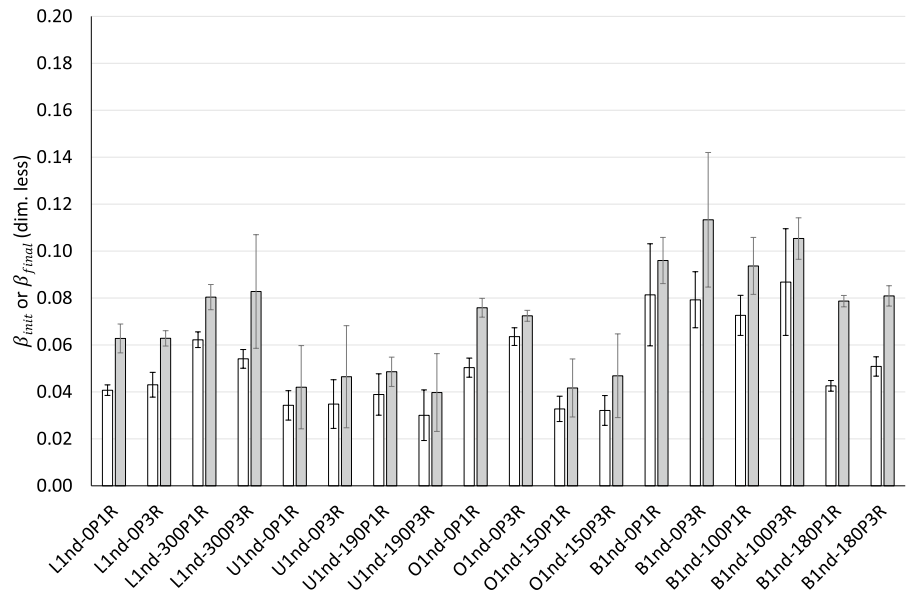
The chemical composition of the used pulps is given in Table 3.

Hygroexpansion measurements were performed to characterize macroscopic changes of the sheets in response to moisture cycling. Figure 1 shows examples of hygroexpansion measurement results for restrained and freely dried samples. The samples shown, L1nd-0P1R and L1nd-0P1F, differed only in the method of drying, L1nd-0P1R was dried with

Table 5 Evaluated parameters from the hygroexpansion measurements for freely dried samples: Initial hygroexpansion coefficient β_{init} , final hygroexpansion coefficient β_{final} , and irreversible shrinkage ϵ_{irr} . Values in brackets are standard deviations

Sample	$\beta_{init}(1)$	$\beta_{final}(1)$	$\epsilon_{irr}(1)$
L1nd-0P1F	0.0748 (0.0116)	0.0764 (0.0135)	0.0005 (0.0003)
L1nd-0P3F	0.0723 (0.0089)	0.0721 (0.0108)	0.0006 (0.0005)
L1nd-300P1F	0.1039 (0.0101)	0.1014 (0.0101)	-0.0010 (0.0009)
L1nd-300P3F	0.0969 (0.0057)	0.0963 (0.0068)	-0.0007 (0.0006)
U1nd-0P1F	0.0744 (0.0087)	0.0721 (0.0091)	0.0002 (0.0002)
U1nd-0P3F	0.0796 (0.0151)	0.0854 (0.0186)	-0.0001 (0.0004)
U1nd-190P1F	0.1003 (0.0205)	0.0979 (0.0247)	0.0000 (0.0018)
U1nd-190P3F	0.1115 (0.0282)	0.1235 (0.0386)	0.0005 (0.0012)
O1nd-0P1F	0.0939 (0.0100)	0.0919 (0.0123)	0.0002 (0.0002)
O1nd-0P3F	0.0897 (0.0119)	0.0887 (0.0141)	-0.0001 (0.0005)
O1nd-150P1F	0.1057 (0.0058)	0.1022 (0.0087)	0.0002 (0.0005)
O1nd-150P3F	0.1090 (0.0093)	0.1057 (0.0097)	-0.0004 (0.0006)
B1nd-0P1F	0.1293 (0.0103)	0.1255 (0.0106)	0.0014 (0.0005)
B1nd-0P3F	0.1400 (0.0064)	0.1233 (0.0061)	0.0008 (0.0003)
B1nd-100P1F	0.1603 (0.0118)	0.1427 (0.0108)	0.0003 (0.0007)
B1nd-100P3F	0.1546 (0.0115)	0.1392 (0.0105)	0.0010 (0.0003)

Fig. 2 Hygroexpansion coefficients measured on sheets dried with restraints. White bars: the initial hygroexpansion coefficients (β_{init}), grey bars: the final hygroexpansion coefficients (β_{final}). The error bars indicate standard deviations



restraints and L1nd-0P1F was dried freely. Sample L1nd-0P1R shows a behaviour typical for paper material dried with restraints, with an initial transient and non-linear behaviour during the first cycle, followed by a stable and close to linear behaviour during subsequent cycles. There is a difference in hygroexpansive strain (ϵ) between the curve during the first cycle and subsequent cycles. The change in hygroexpansive strain from the starting point at 50% RH and

the final point at 50% RH is the irreversible shrinkage ϵ_{irr} . Sample L1nd-0P1F shows behaviour typical for freely dried paper with a quite stable and almost linear behaviour, even from the beginning of the measurement, and a small irreversible shrinkage. There is also a difference between the slopes of the stable part of the curves, with the curve for the freely dried sample being steeper. This is in accordance with earlier findings (Kajanto and Niskanen 1998).

Fig. 3 Hygroexpansion coefficients measured on freely dried sheets. White bars: the initial hygroexpansion coefficients (β_{init}), grey bars: the final hygroexpansion coefficients (β_{final}). The error bars indicate standard deviations

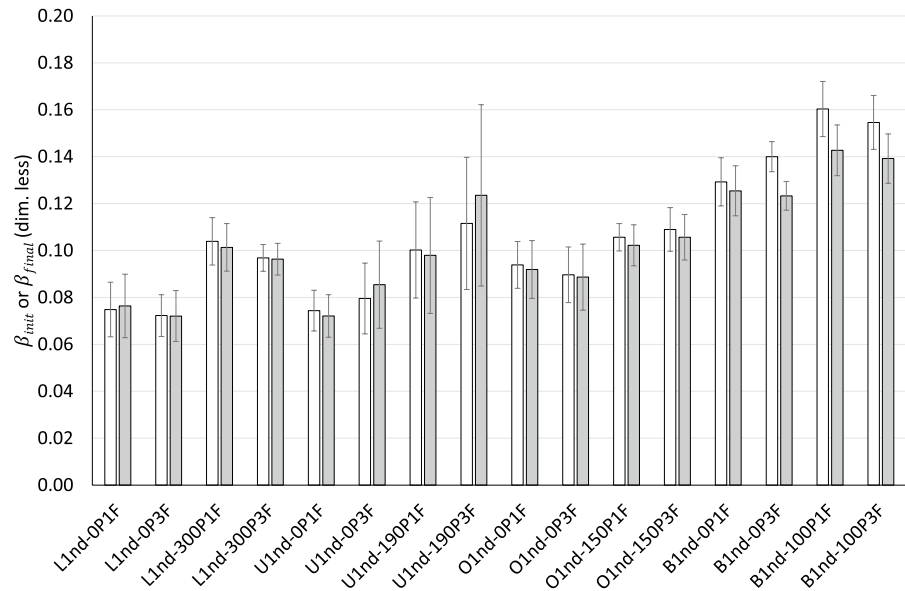
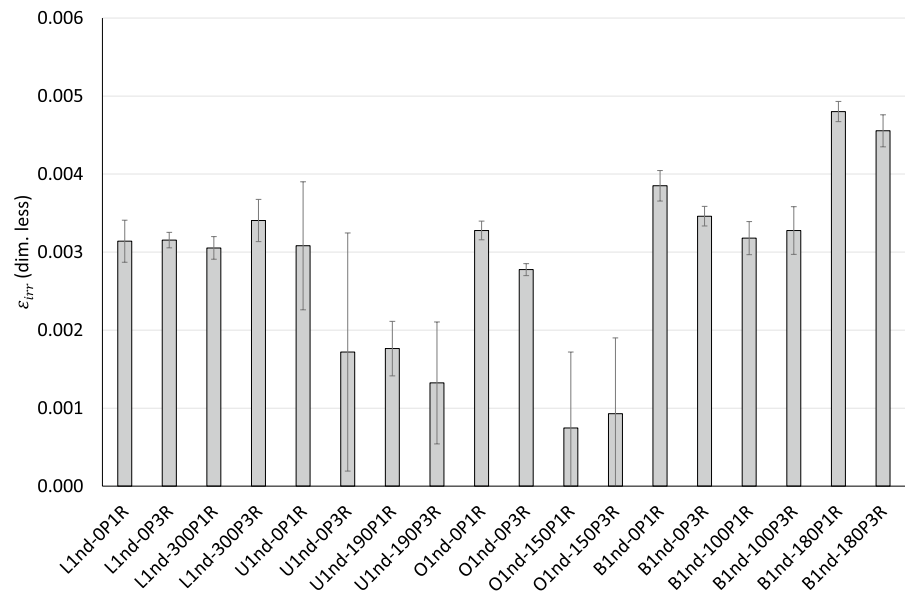


Fig. 4 Irreversible shrinkage (ϵ_{irr}) for sheets dried with restraints. The error bars indicate standard deviations



The hygroexpansion coefficients as defined in this work are the slopes of secants from the leftmost point of the curve (corresponding to 20% RH) to the rightmost point (corresponding to 87% RH) of the first and last cycle. The final hygroexpansion coefficient β_{final} thus corresponds closely to the slope of the stable, almost linear part of the curves, while the initial hygroexpansion coefficient β_{init} could differ significantly from the actual slope of the curve, at least for the restrained dried samples.

The evaluated parameters from the hygroexpansion measurements are presented in Tables 4 and 5 for the restrained and freely dried samples, respectively.

The hygroexpansion coefficients are shown in Figs. 2 and 3. For the sheets dried with restraints, a difference between the initial and final hygroexpansion coefficients is observed, where the latter is always larger due to the transient behaviour of the first cycle. The difference for the freely dried sheets was smaller or insignificant. The hygroexpansion

Fig. 5 Irreversible shrinkage (ϵ_{irr}) for freely dried sheets. The error bars indicate standard deviations

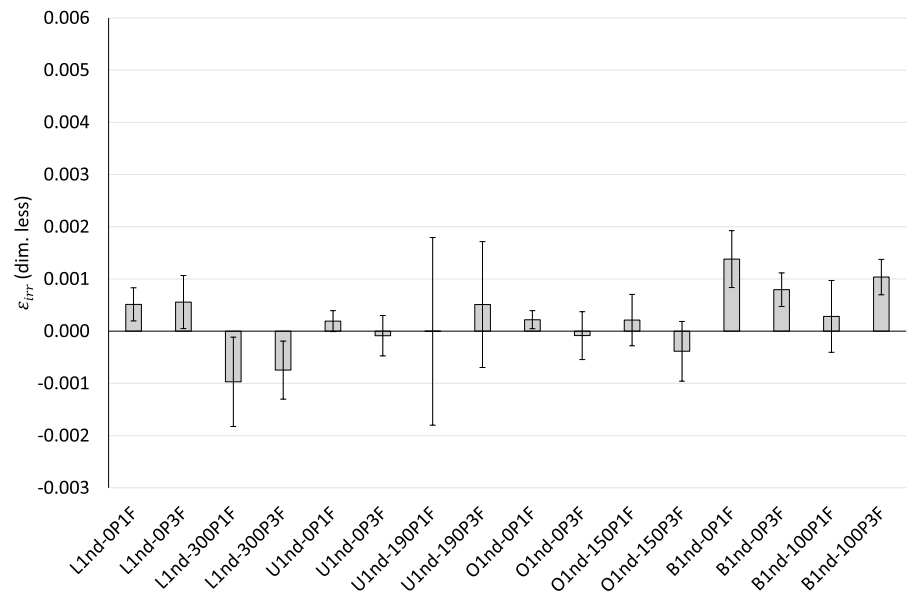
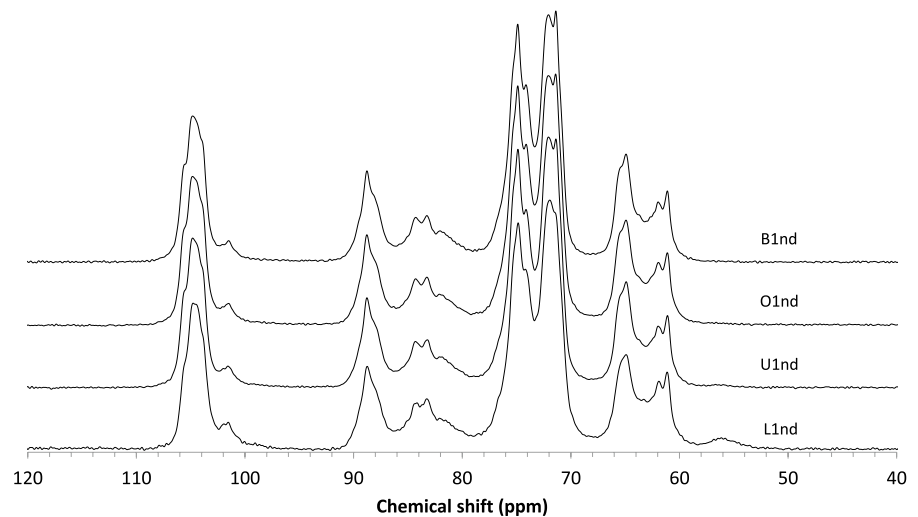


Fig. 6 CP/MAS ^{13}C -NMR spectra recorded on the never-dried (nd) pulps as supplied. Annotations are those given in Table 1



coefficients were typically larger for the freely dried samples.

The irreversible shrinkages are shown in Figs. 4 and 5. For the sheets dried with restraints, there was always an irreversible shrinkage. For the freely dried samples, the irreversible shrinkages were in general, smaller, in some cases even negative, and often of a magnitude that is not statistically significant.

For the hygroexpansion coefficients recorded on sheets dried with restraints, Fig. 2, no systematic

trends were found with respect to treatment extent (press level or degree of beating) between the different pulp types. For example, in the case of both O1nd and B1nd pulps more extensive treatment increased hygroexpansion coefficients, whereas the trend was absent in the U1nd sheets and reversed for L1nd sheets. For the measured irreversible shrinkage, sheets dried with restraints (Fig. 4) showed overall larger magnitudes as compared with the sheets dried freely (Fig. 5), which showed small or close to zero

Table 6 Results from CP/MAS ^{13}C -NMR and WAXS measurements on never-dried (water swollen) pulps

Sample	LFD (nm)	nDCr (%)	CS (nm)	sDCr (%)
L1nd	3.7 (0.1)	48 (3)	5.13 (0.04)	57.9 (0.4)
U1nd	4.2 (0.1)	53 (2)	5.56 (0.04)	60.1 (0.3)
O1nd	4.2 (0.1)	53 (2)	5.70 (0.05)	60.8 (0.4)
B1nd	4.5 (0.2)	56 (3)	5.82 (0.06)	61.3 (0.4)

LFD and nDCr are the average lateral fibril dimensions and the degree of cellulose crystallinity obtained from CP/MAS ^{13}C -NMR spectra, respectively. CS and sDCr are the average crystallite size and degree of crystallinity obtained from WAXS diffractograms, respectively

magnitudes. Among the sheets dried with restraints no systematic trends with respect to press level,

degree of beating or chemical composition of the pulps (Table 3) was observed.

CP/MAS ^{13}C -NMR and WAXS data were recorded on the never dried pulps for the purpose of characterizing the fibre wall nanostructure in the water swollen state.

The CP/MAS ^{13}C -NMR spectra recorded on the never dried pulps are shown in Fig. 6. Apart from the signal clusters originating from cellulose I, signals from hemicelluloses can be seen at about 102 ppm and 82 ppm. In the spectrum recorded on the L1nd sample, due to its higher lignin content, an additional signal origination from lignin is visible at about 56 ppm.

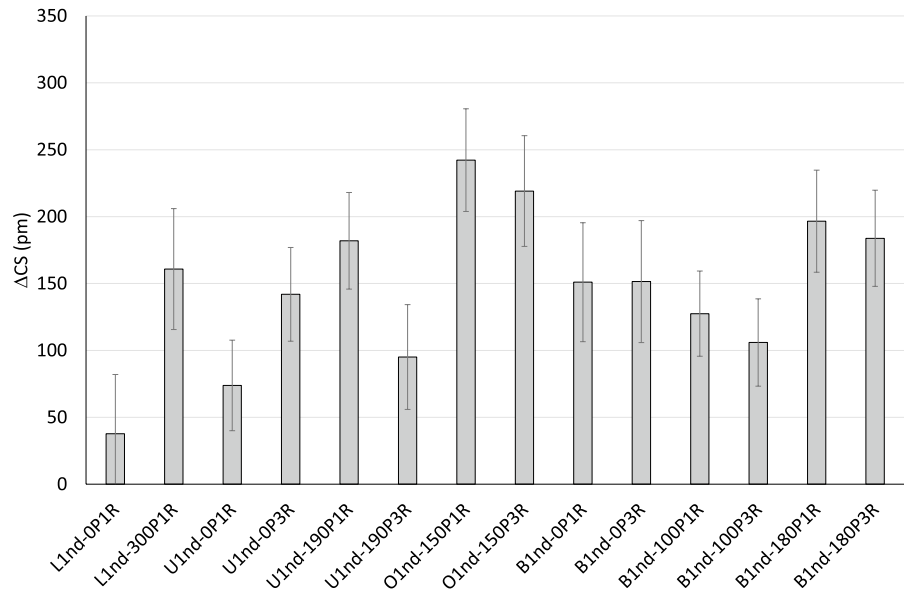
In Table 6 the average lateral fibril dimensions (LFD) estimated from CP/MAS ^{13}C -NMR data and the crystallite sizes (CS) estimated from WAXS

Table 7 Crystallite size (CS), degree of cellulose crystallinity (sDCr) and, changes resulting from moisture cycling (ΔCS and ΔsDCr) determined by WAXS on samples dried with restraints

Sample	CS (nm)	sDCr (%)	ΔCS (nm)	ΔsDCr (%)
L1nd-0P1R	4.23 (0.03)	Δ 52.4 (0.4)	–	–
L1nd-0P1R_h	4.27 (0.03)	52.7 (0.3)	38 (44)	0.3 (0.5)
L1nd-300P1R	4.25 (0.03)	52.6 (0.4)	–	–
L1nd-300P1R_h	4.42 (0.03)	53.7 (0.3)	161 (45)	1.1 (0.5)
U1nd-0P1R	4.45 (0.02)	53.9 (0.2)	–	–
U1nd-0P1R_h	4.52 (0.02)	54.3 (0.2)	74 (34)	0.5 (0.3)
U1nd-0P3R	4.41 (0.02)	53.6 (0.3)	–	–
U1nd-0P3R_h	4.55 (0.03)	54.5 (0.3)	142 (35)	0.9 (0.4)
U1nd-190P1R	4.42 (0.02)	53.7 (0.3)	–	–
U1nd-190P1R_h	4.60 (0.03)	54.8 (0.3)	182 (36)	1.2 (0.4)
U1nd-190P3R	4.54 (0.03)	54.4 (0.3)	–	–
U1nd-190P3R_h	4.63 (0.03)	55.0 (0.3)	95 (39)	0.6 (0.4)
O1nd-150P1R	4.42 (0.03)	53.7 (0.3)	–	–
O1nd-150P1R_h	4.66 (0.03)	55.2 (0.3)	242 (38)	1.5 (0.4)
O1nd-150P3R	4.51 (0.03)	54.3 (0.3)	–	–
O1nd-150P3R_h	4.73 (0.03)	55.6 (0.3)	219 (41)	1.3 (0.4)
B1nd-0P1R	4.41 (0.03)	53.6 (0.3)	–	–
B1nd-0P1R_h	4.56 (0.03)	54.6 (0.3)	151 (44)	1.0 (0.5)
B1nd-0P3R	4.44 (0.03)	53.8 (0.3)	–	–
B1nd-0P3R_h	4.60 (0.03)	54.8 (0.3)	151 (46)	1.0 (0.5)
B1nd-100P1R	4.50 (0.02)	54.2 (0.2)	–	–
B1nd-100P1R_h	4.63 (0.02)	55.0 (0.2)	127 (32)	0.8 (0.3)
B1nd-100P3R	4.52 (0.02)	54.3 (0.2)	–	–
B1nd-100P3R_h	4.62 (0.02)	55.0 (0.2)	106 (33)	0.7 (0.3)
B1nd-180P1R	4.49 (0.03)	54.1 (0.3)	–	–
B1nd-180P1R_h	4.68 (0.03)	55.3 (0.2)	197 (38)	1.2 (0.4)
B1nd-180P3R	4.52 (0.02)	54.4 (0.3)	–	–
B1nd-180P3R_h	4.71 (0.03)	55.5 (0.2)	184 (36)	1.1 (0.4)

Values in parentheses are standard errors

Fig. 7 Change in cellulose crystallites size (ΔCS) in sheets dried with restraints due to moisture cycling, determined by WAXS. Error bars are standard errors



data, both showed an increasing trend with respect to decreasing lignin content of the pulps (Table 3). For the L1nd pulp, it is possible that the comparatively lower values are an artefact due to its higher lignin content. Since the degrees of crystallinities (nDCr and sDCr) in Table 6 are calculated based on their corresponding LFD and CS values, the correlation between LFD and nDCr, and the correlation between CS and sDCr are given by their respective definitions.

For the purpose of monitoring changes in the fibre wall nanostructure resulting from moisture cycling, CP/MAS ^{13}C -NMR, WAXS and SAXS measurements were performed on some of the test pieces before and after moisture cycling. The test pieces were measured after conditioning at 23 °C and 50% RH, while the moisture content was low during the nanostructure measurements. Further, during the WAXS and SAXS measurements the test pieces were exposed to the beam path vacuum, possibly decreasing the moisture content further.

For the freely dried sheets, low grammage sheets were prepared, representing a sheet with a significantly lower degree of inter-fibre joints. In the tables below this is indicated by the suffix “-T”. The low grammage sheets were subjected to the same moisture cycling as the other test pieces but due to their low grammage, hygroexpansion coefficients and measures of the irreversible shrinkage could not be determined with the equipment used in this study.

Changes in the crystallite sizes given in Table 7 are shown in Fig. 7.

Changes in the crystallite sizes given in Table 8 are shown in Fig. 8.

For sheets dried with restraints and for sheets dried freely, the observed changes in crystallite size were consistently positive (Figs. 7 and 8), an increase in crystallite size resulted when the sample was subjected to moisture cycling. In a few cases changes were positive but not statistically significant, typically this was observed for the samples subjected to low degrees of beating and pressing.

CP/MAS ^{13}C -NMR spectra were recorded on selected samples before and after moisture cycling. After the final cycle in the moisture cycling, conditioning at 23 °C and 50% RH made the moisture content of the samples low, while the spectral resolution in the recorded CP/MAS ^{13}C -NMR spectra were poor and consequently, spectral fitting results obtained from NMR were associated with large uncertainties.

Changes in lateral fibril dimensions given in Table 9 are shown in Fig. 9.

Changes in lateral fibril dimensions given in Table 10 are shown in Fig. 10.

Figures 9 and 10 show that, despite the large uncertainties in the ΔLFD values obtained by CP/MAS ^{13}C -NMR, all averages are positive, like the observation made by WAXS, and moisture cycling results in an increase in the average LFD. The interpretation of the LFD measurements from NMR and

Table 8 Crystallite size (CS), degree of cellulose crystallinity (sDCr) and, changes resulting from moisture cycling (Δ CS and Δ sDCr) determined by WAXS on freely dried samples

Sample	CS (nm)	sDCr (%)	Δ CS (pm)	Δ sDCr (%)
L1nd-0P1F	4.21 (0.03)	52.3 (0.3)	–	–
L1nd-0P1F_h	4.24 (0.03)	52.5 (0.3)	37 (38)	0.3 (0.4)
L1nd-0P3F	4.07 (0.02)	51.3 (0.3)	–	–
L1nd-0P3F_h	4.36 (0.03)	53.3 (0.3)	289 (38)	2.0 (0.4)
L1nd-300P1F	4.17 (0.03)	52.0 (0.3)	–	–
L1nd-300P1F_h	4.40 (0.03)	53.6 (0.3)	232 (42)	1.6 (0.4)
L1nd-300P3F	4.19 (0.03)	52.1 (0.4)	–	–
L1nd-300P3F_h	4.39 (0.03)	53.5 (0.3)	208 (43)	1.4 (0.5)
L1nd-0P4F-T	4.06 (0.03)	51.3 (0.3)	–	–
L1nd-0P4F-T_h	4.19 (0.02)	52.2 (0.3)	130 (35)	0.9 (0.4)
U1nd-190P1F	4.34 (0.03)	53.2 (0.3)	–	–
U1nd-190P1F_h	4.54 (0.03)	54.5 (0.3)	199 (37)	1.3 (0.4)
U1nd-190P3F	4.42 (0.03)	53.7 (0.3)	–	–
U1nd-190P3F_h	4.62 (0.03)	55.0 (0.3)	200 (38)	1.3 (0.4)
O1nd-0P1F	4.33 (0.02)	53.1 (0.2)	–	–
O1nd-0P1F_h	4.51 (0.02)	54.3 (0.2)	199 (45)	1.3 (0.5)
O1nd-0P3F	4.42 (0.02)	53.7 (0.2)	–	–
O1nd-0P3F_h	4.52 (0.02)	54.3 (0.2)	154 (45)	1.0 (0.5)
O1nd-150P1F	4.49 (0.02)	54.2 (0.3)	–	–
O1nd-150P1F_h	4.57 (0.02)	54.7 (0.2)	83 (34)	0.5 (0.3)
O1nd-150P3F	4.40 (0.02)	53.6 (0.2)	–	–
O1nd-150P3F_h	4.58 (0.03)	54.7 (0.3)	175 (35)	1.1 (0.4)
B1nd-100P1F	4.44 (0.02)	53.8 (0.2)	–	–
B1nd-100P1F_h	4.58 (0.02)	54.7 (0.2)	138 (33)	0.9 (0.3)
B1nd-100P3F	4.49 (0.02)	54.1 (0.2)	–	–
B1nd-100P3F_h	4.63 (0.02)	55.0 (0.2)	141 (34)	0.9 (0.3)

Table 8 (continued)

Sample	CS (nm)	sDCr (%)	Δ CS (pm)	Δ sDCr (%)
B1nd-0P4F-T	4.36 (0.02)	53.3 (0.2)	–	–
B1nd-0P4F-T_h	4.48 (0.02)	54.1 (0.2)	120 (30)	0.8 (0.3)

Samples with an annotation containing “-T” are low grammage tissue sheets. Values in parentheses are standard errors

the CS measurements from WAXS was that both are related to lateral dimensions of the fibril, and that qualitative agreement was expected and found.

Comparing, pulp by pulp, the LFD and CS measured on water swollen pulps (Table 6) was larger than what was observed for the conditioned samples (Tables 7, 8, 9 and 10). The interpretation made was that drying can induce distortion in the cellulose I crystal lattice thereby reducing the degree of order manifested as an apparent decrease in LFD and CS, as observed by averaging techniques such as CP/MAS 13 C-NMR and WAXS. This is a commonly observed phenomenon in CP/MAS 13 C-NMR, when comparing spectra recorded on dry (ambiently dried) and water swollen samples, Fig. 11. Beyond first-time drying of plant fibres, the impact on spectra is largely reversible, a spectrum recorded on a dried sample can be made to recover its spectral resolution by recording a spectrum after the sample material has been re-swollen in water.

In Fig. 11, the signals at 89 ppm and 65 ppm originate from the C4 and C6 atom in the anhydroglucose unit in the crystalline core of the fibrils, respectively. A significant difference in line broadening was observed between the dry and water swollen states, a difference that is largely reversible. Since the fibril core is impenetrable for water molecules (crystalline cellulose has a density of about 1500 kg/m³), the interpretation of this phenomenon was that drying stresses distorts the order of the fibril, including the crystalline polymers within the core (bottom spectrum in Fig. 11). Drying stresses can be released during re-swelling in water, yielding a spectrum of higher resolution (top spectrum in Fig. 11).

CP/MAS 13 C-NMR recorded on dry samples cannot be used to obtain measures of the larger cellulose structures, such as the average lateral fibril aggregate dimensions. Small Angle X-ray Scattering (SAXS)

Fig. 8 Change in cellulose crystallites size (ΔCS) in freely dried sheets due to moisture cycling, determined by WAXS. Error bars are standard errors

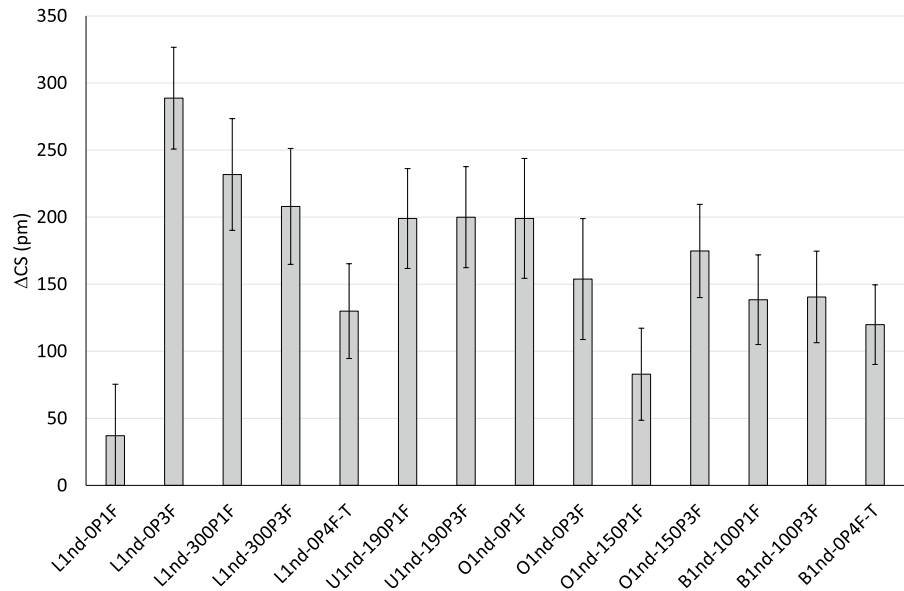
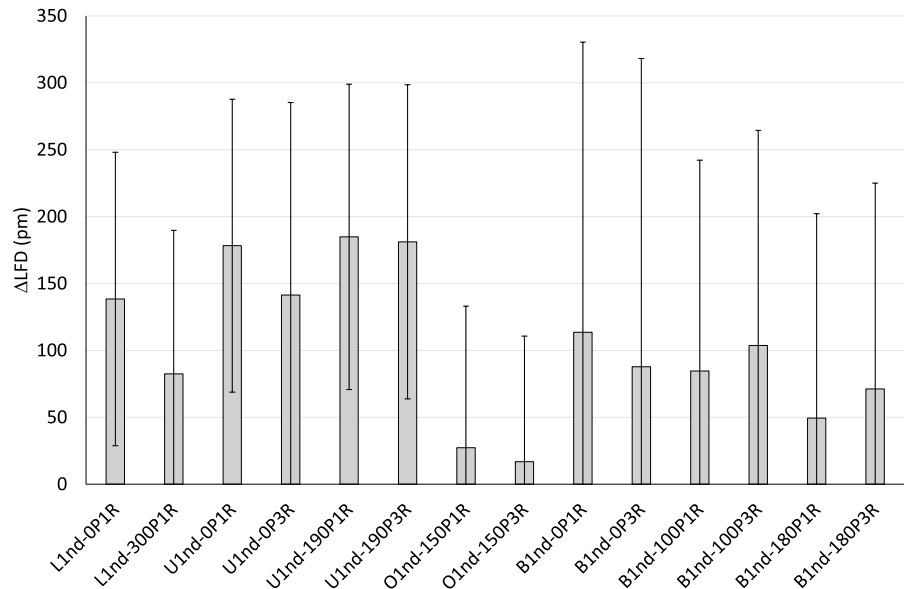


Table 9 Average lateral fibril dimensions (LFD), degree of cellulose crystallinity (nDCr) and, changes resulting from moisture cycling (ΔLFD and $\Delta nDCr$) determined by CP/MAS ^{13}C -NMR on samples dried with restraints. Values in parentheses are standard errors

Sample	LFD (nm)	nDCr (%)	ΔLFD (pm)	$\Delta nDCr$ (%)
L1nd-0P1R	3.4 (0.1)	43.8 (1.6)	–	–
L1nd-0P1R_h	3.5 (0.1)	45.6 (1.7)	138 (110)	1.8 (2.3)
L1nd-300P1R	3.4 (0.1)	44.4 (1.8)	–	–
L1nd-300P1R_h	3.5 (0.1)	45.5 (1.3)	83 (107)	1.1 (2.2)
U1nd-0P1R	3.6 (0.1)	47.0 (0.9)	–	–
U1nd-0P1R_h	3.8 (0.1)	49.0 (1.7)	178 (109)	2.0 (2.0)
U1nd-0P3R	3.7 (0.1)	47.5 (2.4)	–	–
U1nd-0P3R_h	3.8 (0.1)	49.1 (1.7)	141 (144)	1.6 (3.0)
U1nd-190P1R	3.6 (0.1)	47.2 (1.1)	–	–
U1nd-190P1R_h	3.8 (0.1)	49.3 (1.8)	185 (114)	2.1 (2.1)
U1nd-190P3R	3.6 (0.1)	46.8 (1.7)	–	–
U1nd-190P3R_h	3.8 (0.1)	48.9 (1.6)	181 (117)	2.1 (2.4)
O1nd-150P1R	3.7 (0.1)	47.6 (1.5)	–	–
O1nd-150P1R_h	3.7 (0.1)	47.9 (1.5)	27 (106)	0.3 (2.1)
O1nd-150P3R	3.7 (0.1)	47.8 (1.4)	–	–
O1nd-150P3R_h	3.7 (0.1)	47.8 (1.4)	17 (94)	0.2 (1.9)
B1nd-0P1R	3.8 (0.1)	49.1 (2.4)	–	–
B1nd-0P1R_h	3.9 (0.2)	50.3 (3.6)	114 (217)	1.2 (4.3)
B1nd-0P3R	3.8 (0.2)	49.2 (3.1)	–	–
B1nd-0P3R_h	3.9 (0.2)	50.1 (3.6)	88 (230)	0.9 (4.7)
B1nd-100P1R	3.8 (0.1)	49.2 (2.3)	–	–
B1nd-100P1R_h	3.9 (0.1)	50.1 (2.2)	85 (158)	0.9 (3.2)
B1nd-100P3R	3.8 (0.1)	49.2 (2.5)	–	–
B1nd-100P3R_h	3.9 (0.1)	50.3 (2.1)	104 (161)	1.1 (3.3)
B1nd-180P1R	3.8 (0.1)	49.4 (2.3)	–	–
B1nd-180P1R_h	3.9 (0.1)	50.0 (2.1)	49 (153)	0.5 (3.1)
B1nd-180P3R	3.8 (0.1)	48.9 (2.3)	–	–
B1nd-180P3R_h	3.9 (0.1)	49.7 (2.1)	71 (154)	0.8 (3.2)

Fig. 9 Change in cellulose average lateral fibril dimension (Δ LFD) in sheets dried with restraints due to moisture cycling, determined by CP/MAS 13 C-NMR. Error bars are standard errors



can give information on size ranges larger than obtainable by WAXS and CP/MAS 13 C-NMR also in dry samples. SAXS measurements were performed on samples dried with restraints before and after moisture cycling, some examples results are shown below.

Over the size-range covered by the SAXS measurements (correlation lengths of about 1 nm–80 nm) there were significant structural differences between liner samples (L1nd) and the bleached samples (B1nd) for both sheets dried with restraints and freely dried sheets, Figs. 12 and 13. A signal at about 1.5 nm^{-1} is visible in the bleached samples, independent of drying method and remains after moisture cycling. The signal was interpreted as resulting mainly from the removal of lignin between cellulose fibrils and fibril aggregates, thereby creating voids and subsequently more electron density contrast. The signal at 1.5 nm^{-1} corresponds to a correlation length of about 4.2 nm, similar to the range of cellulose crystallite sizes observed by WAXS in the bleached samples, 4.4 nm–4.7 nm (Tables 7 and 8).

The response to moisture cycling observed by SAXS was small or negligible for the sheets dried with restraints, with a small decrease in the signal intensity range from 0.4 nm^{-1} to 1 nm^{-1} (correlation lengths of about 16 nm to 6 nm) as a result of moisture cycling in the B1nd-100P3R sample in Fig. 12. The interpretation made was that the structural changes induced by moisture cycling in the

B1nd-100P3R sample mainly decreased the abundance of structures in the size range typical of cellulose fibril aggregates and any associated pore system, possibly resulting in a compacting over the affected size range. The result shown in Fig. 12 was typical for the SAXS data recorded on sheets dried with restraints, and due to the smallness of changes induced by moisture cycling, no systematic trends were obvious.

For SAXS measurements performed on freely dried sheets, measurements on the low grammage sheets were used for comparisons, Fig. 13. The liner sheets (L1nd-0P4F-T and L1nd-300P1F) showed small responses to moisture cycling, at the low q -value range (larger structures). The low grammage sheet indicated a lower abundance of large-scale structures in response to moisture cycling whereas the L1nd-300P1F showed an increase in signal intensity at low q -values as a response to moisture cycling. The L1nd-300P1F also showed a small decrease in the signal intensity range from 0.4 nm^{-1} to 1 nm^{-1} like the B1nd-100P3R sheets dried with restraints (lower right panel in Fig. 12). For the freely dried sheets, Fig. 13, no significant changes in response to moisture cycling were observed in SAXS data recorded on the low-grammage sheet made from bleached pulp, B1nd-0P4F-T. The B1nd-100P3F sample showed similar changes as found for its counterpart dried with restraints (B1nd-100P3R in Fig. 12) but more pronounced in the case of the

Table 10 Average lateral fibril dimensions (LFD), degree of cellulose crystallinity (nDCr) and, changes resulting from moisture cycling (Δ LFD and Δ nDCr) determined by CP/MAS 13 C-NMR on freely dried samples. Samples with an annotation containing “-T” are low grammage tissue sheets. Values in parentheses are standard errors

Sample	LFD (nm)	nDCr (%)	Δ LFD (pm)	Δ nDCr (%)
L1nd-0P1F	3.4 (0.1)	43.7 (1.3)	–	–
L1nd-0P1F_h	3.4 (0.1)	44.0 (1.3)	26 (83)	0.4 (1.8)
L1nd-0P3F	3.4 (0.1)	44.0 (1.1)	–	–
L1nd-0P3F_h	3.4 (0.1)	44.1 (1.2)	8 (78)	0.1 (1.6)
L1nd-300P1F	3.4 (0.1)	43.8 (1.3)	–	–
L1nd-300P1F_h	3.4 (0.1)	44.8 (1.2)	73 (85)	1.0 (1.7)
L1nd-300P3F	3.4 (0.0)	43.8 (1.0)	–	–
L1nd-300P3F_h	3.5 (0.1)	45.2 (1.2)	103 (76)	1.3 (1.5)
L1nd-0P4F-T	3.4 (0.1)	44.3 (1.6)	–	–
L1nd-0P4F-T_h	3.5 (0.1)	45.5 (1.4)	89 (103)	1.1 (2.1)
U1nd-190P1F	3.7 (0.1)	48.0 (1.7)	–	–
U1nd-190P1F_h	3.8 (0.1)	49.3 (1.8)	116 (126)	1.3 (2.5)
U1nd-190P3F	3.7 (0.1)	47.7 (1.5)	–	–
U1nd-190P3F_h	3.8 (0.1)	49.4 (2.0)	148 (126)	1.7 (2.5)
B1nd-100P1F	3.8 (0.1)	48.6 (2.1)	–	–
B1nd-100P1F_h	3.9 (0.1)	50.0 (2.1)	125 (148)	1.4 (3.0)
B1nd-100P3F	3.7 (0.1)	48.4 (2.1)	–	–
B1nd-100P3F_h	3.9 (0.1)	49.9 (2.3)	137 (153)	1.5 (3.1)
B1nd-0P4F-T	3.8 (0.1)	48.5 (2.2)	–	–
B1nd-0P4F-T_h	3.9 (0.1)	50.2 (2.2)	150 (157)	1.6 (3.2)

freely dried sheet. Although the responses to moisture cycling could be discerned between extreme sheets (extreme with respect to grammage, press levels, and degrees of beating) no clear systematic trends in SAXS data were immediately obvious for the freely dried samples.

To find if any correlation existed between the measured structural changes, observed in response moisture cycling, on the nano and macroscale, the macroscopic hygroexpansion measures were charted against changes in the crystallite sizes determined by WAXS.

For the sheets dried with restraints no correlations were found between either the irreversible shrinkage or the final hygroexpansion coefficients and the change in crystallite sizes, Figs. 14 and 15. In the case of change in crystallite size charted against irreversible shrinkage (Fig. 14) the L1nd-0P1R and L1nd-300P1R samples showed the same ϵ_{irr} but were associated with a significant difference in Δ CS, Fig. 14. Further, among the bleached samples (B1nd) differences were observed in ϵ_{irr} and in the average values of Δ CS but no systematic trend with respect to press-levels of degree of beating was observed.

For the freely dried sheets, the irreversible shrinkage was small and, in most cases, not statistically significant. The final hygroexpansion coefficient for freely dried sheets, showed no correlation with the change in crystallite sizes, Fig. 16.

During moisture cycling, Δ CS values calculated from WAXS data and Δ LFD values calculated from CP/MAS 13 C-NMR data were consistently positive for sheets dried with restraints and for sheets dried freely (Figs. 7, 8, 9 and 10). The interpretation made here was that moisture cycling leads to an average increase in the local order in cellulose fibrils/crystallites as a result of some form of structural relaxation e.g., relaxation of local stress concentrations.

The sheets dried with restraints showed significant irreversible strains, Fig. 4, contrary to the sheets that were dried freely, Fig. 5. For both sheets dried with restraints and freely, the change in crystallite sizes were of similar magnitudes independent of drying method, Figs. 7 and 8. The impact of restrained drying seems unconnected to structural changes on the nanoscale.

For the freely dried sheets, Fig. 8, the low grammage sheets (L1nd-0P4F-T and B1nd-0P4F-T), with fewer inter-fibre joints than the higher grammage sheets, show Δ CS in response to moisture cycling that were of a similar magnitude as in the higher grammage sheets, which makes the inter-fibre joints less likely as the main cause for the observed differences in Δ CS.

Fig. 10 Change in cellulose average lateral fibril dimension (Δ LFD) in freely dried sheets due to moisture cycling, determined by CP/MAS 13 C-NMR. Error bars are standard errors

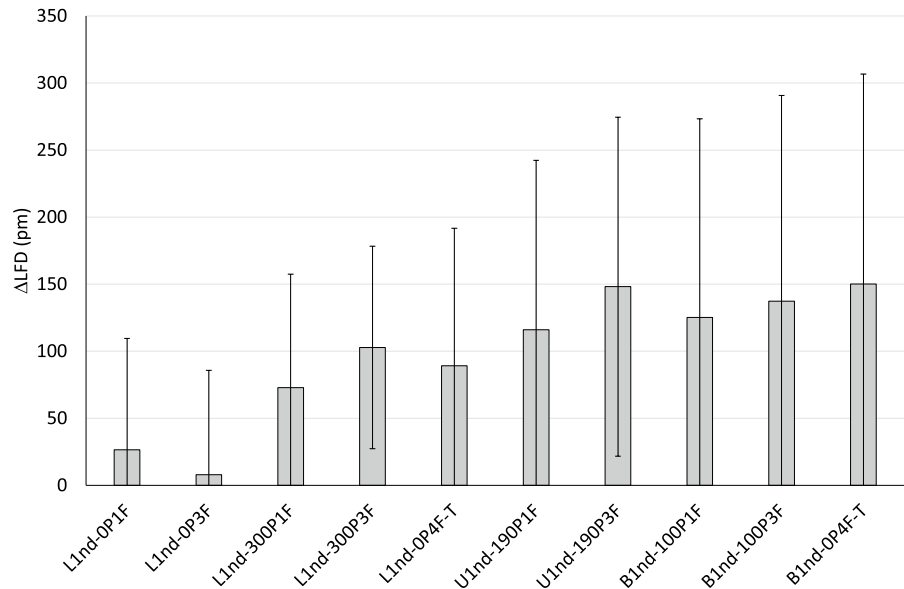
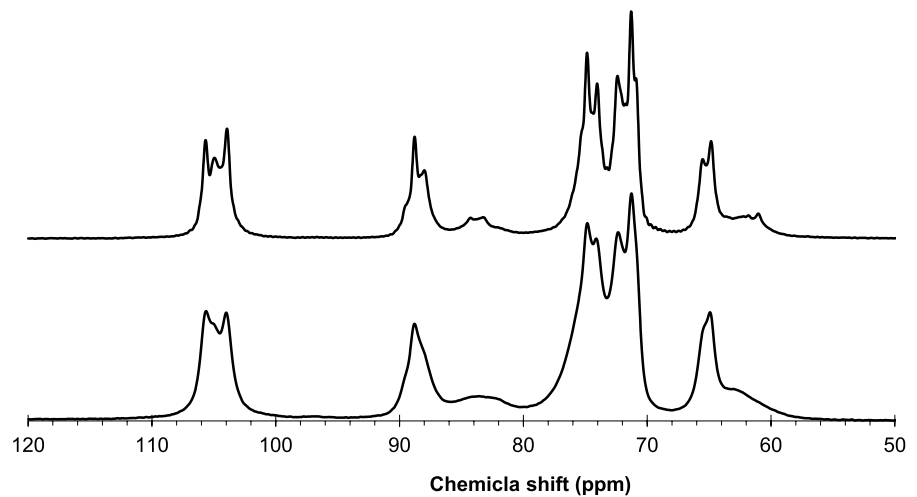


Fig. 11 CP/MAS 13 C-NMR spectra recorded on cotton linters, top: water swollen, bottom: ambiently dried. The difference in spectra is mainly reversible, spectra look similar for repeated measurements when cycling the sample material between dry and water swollen states



As shown by Uesaka (Uesaka et al. 1994) the out-of-plane configurations of the inter-fibre joints (fiber-to-fiber bonds) can increase the hygroexpansion dramatically. The out-of-plane configurations are more prevalent in the freely dried sheets. This agrees with the findings in this work, the freely dried sheets showed typically larger magnitudes for the hygroexpansion coefficients than the sheets dried with restraints, Figs. 2 and 3.

This could also give a clue about the lack of correlations between macro and nanoscale measurement result. If changes in nanoscale structure due

to moisture cycling (Δ CS) occurs throughout the entirety of the fibre wall with similar magnitude and character independent of the proximity to an inter-fibre joint (the “out-of-plane configurations”), no significant differences in Δ CS would be expected because of the abundance or extent of the inter-fibre joints.

This agrees with the observations for the low-grammage sheets which showed Δ CS magnitudes similar to those of the higher grammage sheets, Fig. 8, and agrees with the finding that Δ CS showed

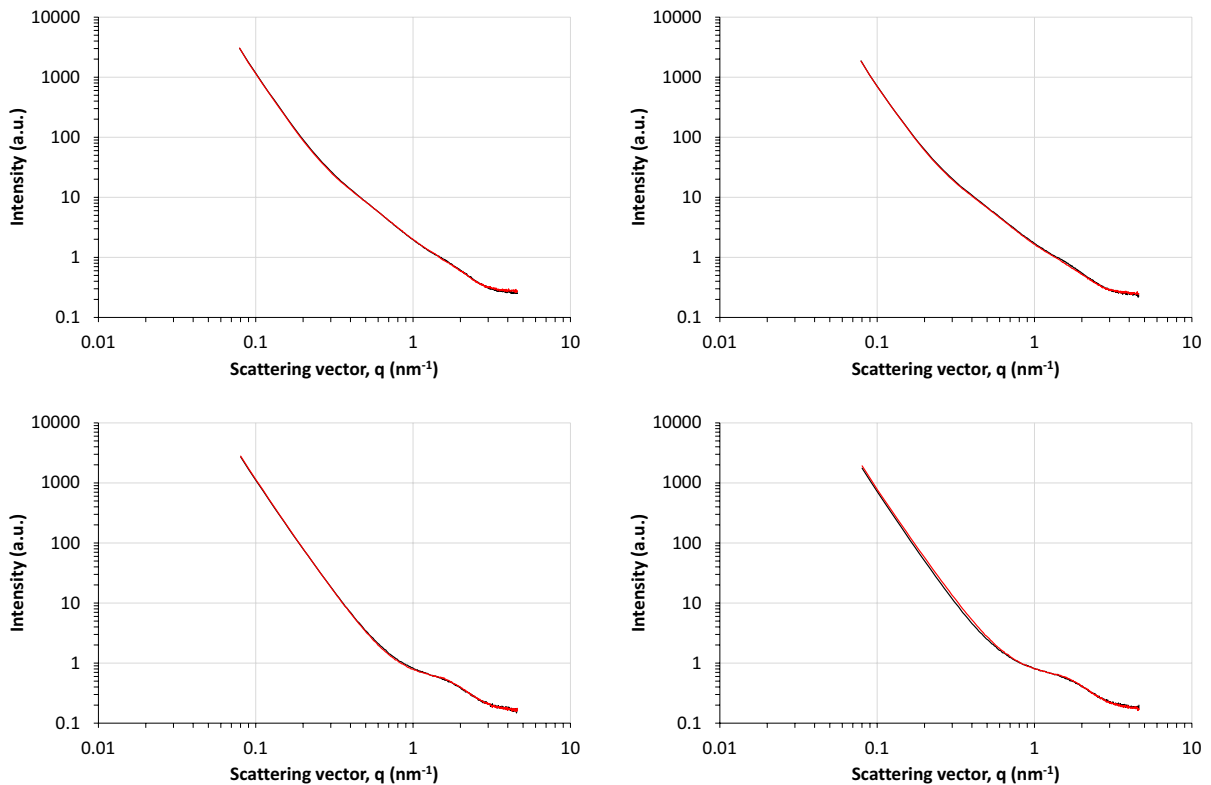


Fig. 12 SAXS data recorded on sheets dried with restraints, top left: L1nd-0P1R, top right: L1nd-300P1R, bottom left: B1nd-0P1R, bottom right: B1nd-100P3R. In each panel SAXS data recorded before (black) and after (red) moisture cycling are superimposed

similar magnitudes for sheets dried with restraints and sheets dried freely, Figs. 7 and 8.

In an idealized structure model of a pulp fibre wall with cellulose arranged into fibril aggregates, sorbed water moisture can accumulate/reside in two places; in smaller interstitial cavities between cellulose fibrils within an aggregate, and in larger cavities (pores) between aggregates. During moisture sorption water molecules accumulated between aggregates is the main cause for the change in macroscopic dimensions (i.e. swelling), while water molecules penetrating into the aggregate interior are mainly responsible for releasing stress concentrations, causing the structural relaxation that is manifested in the signal narrowing observed by both NMR and X-ray. If, during moisture sorption, water penetration into aggregate interiors precedes the accumulation of water between aggregates, release of stress concentrations would occur already at low moisture contents. This would effectively decouple the release of stress concentrations from any further swelling resulting from an

increased accumulation of water between aggregates. Such behaviour has been observed by x-ray scattering measurements performed on wood, exposed to different relative humidities. Measurements showed that crystallite deformations occurred and fibre bundle swelling, took place at different moisture contents, with crystallite deformations most pronounced at lower moisture content (Paajanen 2022). This was the suggested explanation for the lack of correlation between the macro and nanoscale changes observed in response to moisture cycling.

Conclusions

Hygroexpansion, CP/MAS ^{13}C -NMR, WAXS and SAXS measurements were made on sheets made from four different commercial pulps of different lignin content. Non-directional laboratory sheets were made from the pulps with different degrees of beating and were prepared at different press levels. The sheets were dried

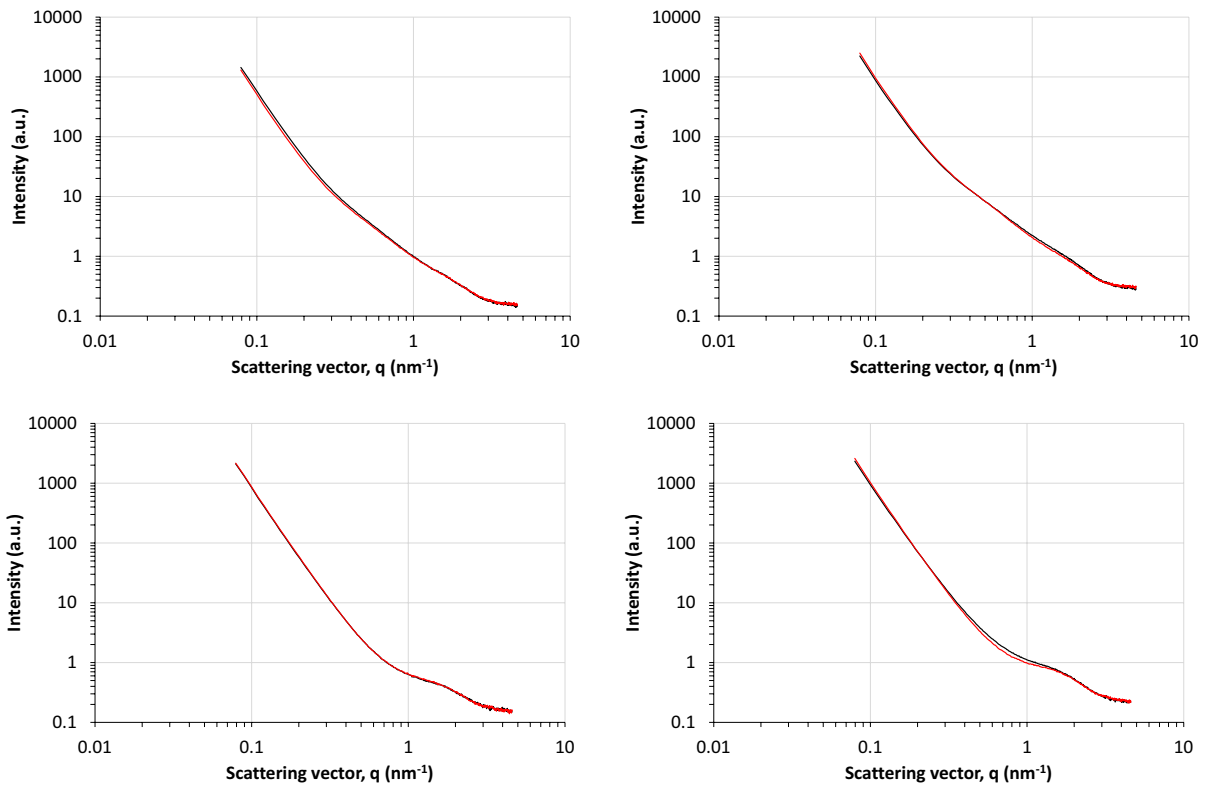


Fig. 13 SAXS data recorded on freely dried sheets, top left: L1nd-0P4F-T, top right: L1nd-300P1F, bottom left: B1nd-0P4F-T, bottom right: B1nd-100P3F. In each panel SAXS data recorded before (black) and after (red) moisture cycling are superimposed

Fig. 14 Nanoscale vs. macroscale measurement results for sheets dried with restraints. The change in cellulose crystallite size (ΔCS) charted against the irreversible shrinkage (ϵ_{irr}). Data and error estimates are based on common data in Tables 4 and 7

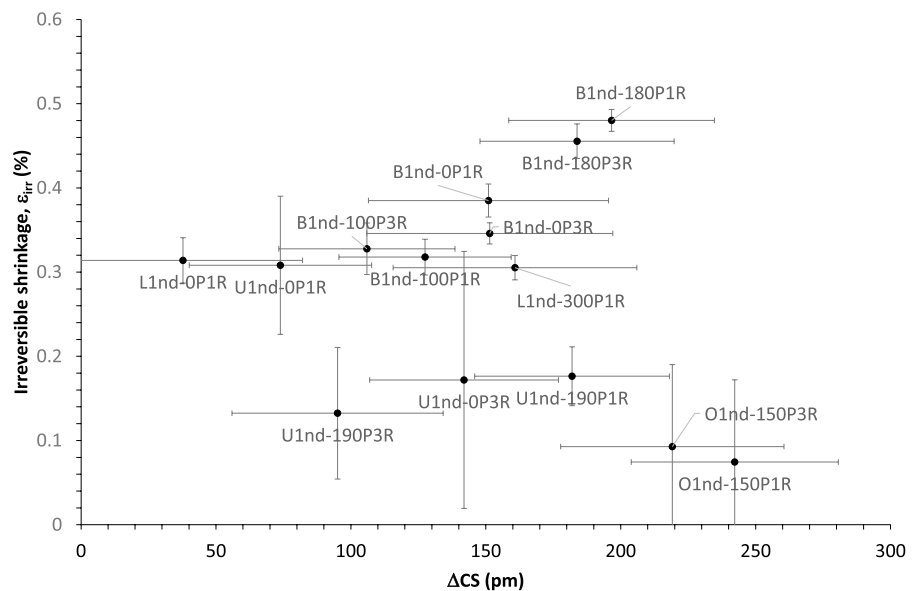


Fig. 15 Nanoscale vs. macroscale measurement results for sheets dried with restraints. The change in cellulose crystallite size (ΔCS) charted against the final hygroexpansion coefficient (β_{final}). Data and error estimates are based on common data in Tables 4 and 7

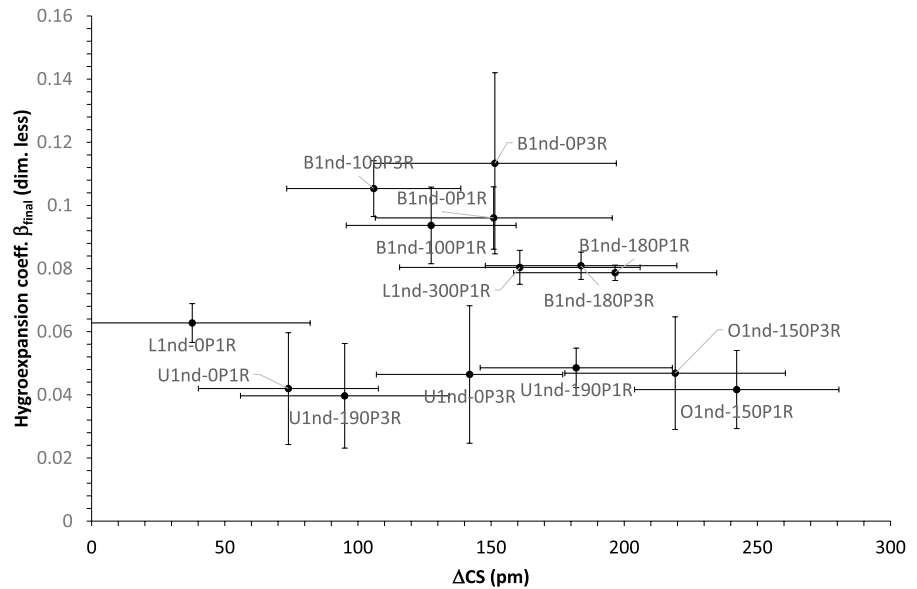
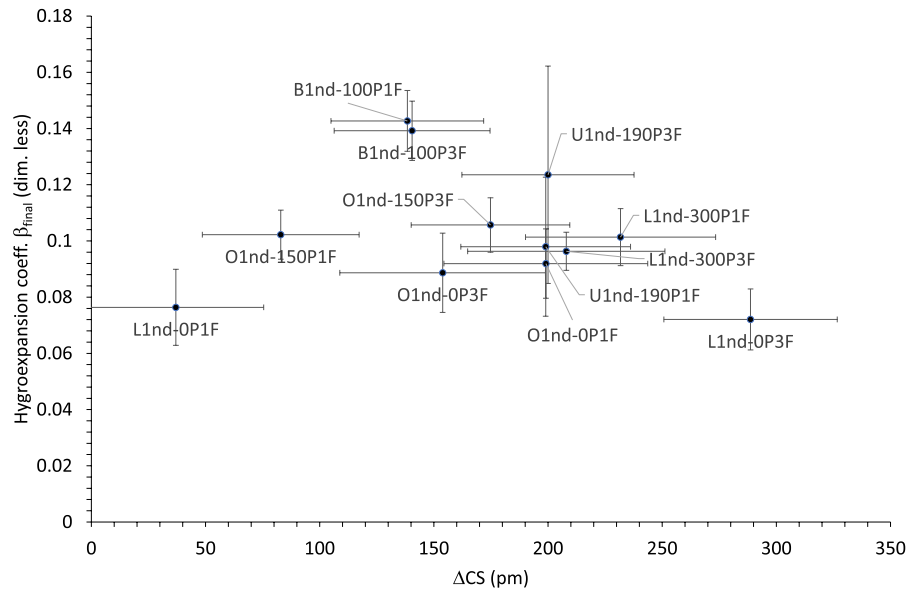


Fig. 16 Nanoscale vs. macroscale measurement results for freely dried sheets. The change in cellulose crystallite size (ΔCS) charted against the final hygroexpansion coefficient (β_{final}). Data and error estimates are based on common data in Tables 5 and 8



freely or with restraints. Measurements were made on sheets before and after moisture cycling to determine hygroexpansion coefficients, changes in cellulose average lateral fibril dimensions and average cellulose crystallite sizes with the aim of elucidating macroscale and nanoscale changes as the result of moisture cycling.

For the sheets consistent and statistically significant structural changes were observed on both macro and nanoscale. On the macroscale, moisture cycling consistently induced irreversible shrinkage in sheets dried with restraints, but less so in the case of sheets

dried freely. The hygroexpansion coefficients were typically higher for freely dried sheets compared with sheets dried with constraints. On the nanoscale moisture cycling consistently induced an increase in the average crystallite sizes (WAXS) and the average lateral fibril dimensions (CP/MAS ^{13}C -NMR) though in the latter case with poor statistical significance. This was interpreted as an increase in the degree of order in the cellulose fibril interior/cellulose crystallite. There were no profound differences in the nanoscale changes observed for sheets dried with restraints and

for sheets dried freely. Changes in the fibre wall nanostructure were of similar magnitude when comparing freely dried sheets with low grammage (less abundant inter-fibre joints) and sheets with higher grammage (more abundant inter-fibre joints). No obvious correlations were found between the macroscale and nanoscale measurements. The proposed explanation for this was that the nanoscale structural changes occurred similarly throughout the entirety of the fibre wall, independent of the proximity to an inter-fibre joint, and that the nanoscale structural changes were mainly the result of water penetrating into the interior of cellulose fibril aggregates.

Acknowledgments The Bioeconomy Research Board is gratefully acknowledged for funding the project “Water induced changes in pulp fibre materials—the microscopic causes for hygroexpansion”. Personnel from Stora Enso, Billerud, Södra and Holmen as well as representatives for Intressentföreningen Packforsk, and STFI’s intressentförening are gratefully acknowledged for helpful discussions and continuous in-kind support to the project work. Dr. Michael Reid is gratefully acknowledged for language revision.

Author contributions All co-authors, PTL, JA, GS, CH have been involved in the development of the project ideas and writing up the application. PTL: Responsible for CP/MAS ^{13}C -NMR, WAXS and SAXS measurements, handling, compilation and interpretation of measurement data. Main writer of the manuscript. JA: Hygroexpansion measurements, handling, compilation and interpretation of measurement data. Writing of manuscript. GS: Pulp handling, treatment and wet chemical characterization. Writing of manuscript. CH: Pulp treatments, preparation of sheet samples, development of drying methods. Writing of manuscript.

Funding Open access funding provided by RISE Research Institutes of Sweden. The Bioeconomy Research Board is gratefully acknowledged for funding the project “Water induced changes in pulp fibre materials—the microscopic causes for hygroexpansion”. Stora Enso, Billerud, Södra and Holmen as well as representatives for Intressentföreningen Packforsk, and STFI’s intressentförening are gratefully acknowledged for helpful discussions and continuous in-kind support to the project work.

Data availability Can be supplied by corresponding author on request.

Declarations

Conflict of interest The authors does not have any conflict of interest to declare

Ethical approval No ethical conflicts exist.

Humans or animal participants Not applicable.

Consent to participate All authors of this manuscript have participated in the work willingly.

Consent for publication All authors of this manuscript give their consent to publish the presented manuscript.

Open Access This article is licensed under a Creative Commons Attribution 4.0 International License, which permits use, sharing, adaptation, distribution and reproduction in any medium or format, as long as you give appropriate credit to the original author(s) and the source, provide a link to the Creative Commons licence, and indicate if changes were made. The images or other third party material in this article are included in the article’s Creative Commons licence, unless indicated otherwise in a credit line to the material. If material is not included in the article’s Creative Commons licence and your intended use is not permitted by statutory regulation or exceeds the permitted use, you will need to obtain permission directly from the copyright holder. To view a copy of this licence, visit <http://creativecommons.org/licenses/by/4.0/>.

References

- FAO, food and agriculture organization of The United Nations (2017), Pulp and paper capacities, survey 2016–2021, Rome, Italy, ISSN 0255–7665 available at URL:<http://www.fao.org/forestry/statistics/80571/en/>.
- Fengel D, Wegener G (1989) Chapters 2 and Chapter 4 in Wood. Chemistry, ultrastructure reactions. Walter de Gruyter, Berlin
- Jansson J (1974) Faserforschung und Textiltechnik 25 Heft 9, Zeitschrift für Polymerforschung.
- Kajanto I, Niskanen K (1998) Dimensional stability. Paper physics. In: Niskanen K (ed) Papermaking science and technology series. Fapet Oy, Helsinki
- Krässig HA (1993) Cellulose. Structure, Accessibility and Reactivity, Polymer Monographs Vol. 11, Gordon and Breach Science, Publishers S.A., Y-Parc, Chemin de la Sallez, Yverdon, Switzerland.
- Larsson PT, Wickholm K, Iversen T (1997) A CP/MAS ^{13}C -NMR investigation of molecular ordering in celluloses. Carbohydr Res 302:19–25. [https://doi.org/10.1016/S0008-6215\(97\)00130-4](https://doi.org/10.1016/S0008-6215(97)00130-4)
- Niskanen K, Kärenlampi P (1998) In-plane tensile properties. Paper physics. In: Niskanen K (ed) Papermaking Science and Technology series. Fapet Oy, Helsinki
- Paajanen A, Zitting A, Rautkari L, Ketoja JA, Penttilä PA (2022) Nanoscale mechanism of moisture-induced swelling in wood microfibril bundles. Nano Lett 22:5143–5150. <https://doi.org/10.1021/acs.nanolett.2c00822>
- Spalla O (2002) General theorems in small-angle scattering neutrons, X-rays and light: scattering applied to soft condensed matter. In: Lindner P, Zemb TH (eds) North-Holland Delta Series. Elsevier, Amsterdam, pp 49–71
- Toba K, Yamamoto H, Yoshida M (2013) Crystallization of cellulose microfibrils in wood cell wall by repeated

dry-and-wet treatment, using X-ray diffraction technique. *Cellulose* 20:633–643. <https://doi.org/10.1007/s10570-012-9853-7>

Uesaka T, Qi D (1994) Hygroexpansivity of paper: effects of fibre-to-fibre bonding. *J Pulp Pap Sci* 20(6):J175–J179

Wickholm K, Larsson PT, Iversen T (1998) Assignment of non-crystalline forms in cellulose I by CP/MAS ^{13}C -NMR spectroscopy. *Carbohyd Res* 312:123–129. [https://doi.org/10.1016/S0008-6215\(98\)00236-5](https://doi.org/10.1016/S0008-6215(98)00236-5)

Publisher's Note Springer Nature remains neutral with regard to jurisdictional claims in published maps and institutional affiliations.